Available online at BCREC website: https://journal.bcrec.id/index.php/bcrec

Bulletin of Chemical Reaction Engineering & Catalysis, 19 (1) 2024, 1-14

Research Article

Tailoring MOF-5 Photocatalysts: Low-Temperature Synthesis and Solvent Variations for Enhanced Performance in Dye Degradation

Himanshi Gupta[1], Isha Saini[1,*], Vinamrita Singh[2], Tanuj Kumar[3], Varsha Singh[4]

[1]Department of Applied Science, School of Engineering and Technology, Sushant University, Gurugram, Haryana, India.
[2]Department of Physics, Netaji Subhas University of Technology, East Campus, Delhi, India.
[3]Department of Nanoscience and Materials, Central University of Jammu, Jammu, India.
[4]Centre for Life Sciences, Chitkara School of Health Sciences, Chitkara University, Rajpura - 140401, Punjab, India.

Received: 26th October 2023; Revised: 4th December 2023; Accepted: 5th December 2023
Available online: 8th December 2023; Published regularly: April 2024

Abstract

Metal-organic frameworks (MOFs) are emerging as pivotal porous crystalline materials with diverse applications. Typically, MOFs are synthesized using solvothermal techniques at high temperatures and pressures. In this study, a novel approach was employed to synthesize zinc-based MOFs, specifically MOF-5, at low temperatures (up to 50 °C) via chemical mixing at standard pressures. Varying the temperature and solvents, N-methyl-2-pyrrolidone (NMP) and N,N-dimethylformamide (DMF), in the chemical mixing process, the highest yield of the material was observed with DMF at 50 °C (M1). Two additional samples, M2 and M3, are synthesized at room temperature using DMF and NMP, respectively. Despite similarities in XRD, Raman, and FTIR analyses confirming successful MOF-5 formation, noticeable differences in sample morphology arise due to distinct synthesis conditions, particularly solvent and temperature variations. The MOF-5 samples exhibit UV absorption with varying band gaps. Notably, when employed as photocatalysts for organic dye (methylene blue) degradation, M2 outperforms others, achieving an impressive 85% degradation under simulated solar light irradiation. This work underscores the significance of tuning MOF photocatalyst properties through tailored synthesis routes, recognizing the profound impact of morphology and elemental composition on enhancing photocatalytic dye degradation performance.

Keywords: Photocatalysis; MOF-5; organic dye degradation; synthesis parameters; water treatment

How to Cite: H. Gupta, I. Saini, V. Singh, T. Kumar, V. Singh (2024). Tailoring MOF-5 Photocatalysts: Low-Temperature Synthesis and Solvent Variations for Enhanced Performance in Dye Degradation. *Bulletin of Chemical Reaction Engineering & Catalysis*, 19 (1), 1-14 (doi: 10.9767/bcrec.20062)

Permalink/DOI: https://doi.org/10.9767/bcrec.20062

1. Introduction

Industrial waste like synthetic dyes, solvents, and germicides are discharged directly into water bodies causing severe water pollution and health hazards to the living organisms. Organic dyes are major pollutants due to their abundant use in textile, plastic, food and paper printing industries [1]. Worldwide production of synthetic dyes is estimated to be 700,000 tons per year and about 10-15% of dyestuff is discharged into water bodies [2–4]. Therefore, removal of dye pollutants from water is a prime concern and methods like adsorption [5,6] and photocatalysis [7], are applied for water purification. Yet the effective removal of dyes from

* Corresponding Author.
Email: isha.saini32@gmail.com (I. Saini)

wastewater is still a challenging task and continues to interest scientists, especially at the advent of nanotechnology.

Degrading organic pollutants by photocatalysis is a simple, effective and inexpensive method. Proper bandgap lying in the visible range, large surface area, stability in aqueous medium, reusability and morphology are some of the important parameters for a material to be a good photocatalyst. When the photocatalytic material is exposed to UV-Visible light radiation, electron and hole pairs are generated. Thereafter, oxidation and reduction reactions occur on the surface of the photocatalyst to create OH^- and superoxide radicals [8]. The organic pollutant is detoxified by these two reactive species [9]. New photocatalytic materials are being constantly explored for efficient, nontoxic and cost-effective degradation of pollutants.

Metal organic frameworks (MOF) are emerging as an important group of porous, crystalline materials finding potential use in photocatalytic process due to their high surface area and green conversion of organic contaminants [10–12]. MOFs are a type of crystalline material having structural periodicity and moderately bonded through coordination bonds. MOFs can be tuned for the desirable pore sizes and shapes by selecting suitable metal centers and organic linkers for specific application [13,14]. The MOFs, based on Zn, Co, Cu, Fe, Al, Zr, Mn, Ni, Cd, Ti, Cr, Ce, and their combinations as bi-metallics, have been explored for degradation of both anionic and cationic dyes [15]. When these materials are irradiated by energy higher than their bandgap, electron-hole pairs are created. The photogenerated electron in the conduction band (CB) reacts with O_2 molecule forming superoxide anion (O_2^-), while the hole in the valence band (VB) reacts with OH^- to form •OH. These O_2^- and •OH species degrade organic dye into harmless products [16].

Cu and Co-based MOF material have been synthesized for degrading methylene blue (MB). The two materials displayed great photocatalytic activity achieving 93.93% degradation of MB by Cu-MOF while 54.70% degradation by Co-MOF after 150 min of visible light irradiation [17]. In another work, the synthesis of Zn(2)-based 3D MOF was done by solvothermal method using polynuclear zinc clusters and 1,4-naphthalene dicarboxylic acid linker. This unique MOF structure showed degradation efficiency of 78.3% for methyl violet (MV) and 56.8% for rhodamine B (RhB) after 40 min of UV irradiation [18]. Ni-based MOFs have been used for the decomposition of crystal violet as well under illumination [19]. About 93% of crystal violet degraded in 30 min of irradiation, thereby depicting the application of MOFs for decomposing a variety of water polluting dyes.

MOF-5, which is a Zn-based MOF, is an interesting material of choice for photocatalytic degradation and has been widely used. However, factors like solvent choice, temperature, and duration of reaction for synthesis process can significantly impact its structural properties, surface area, porosity, and ultimately its photocatalytic performance. The choice of solvent used during MOF-5 synthesis can influence the nucleation and hence crystal growth process along with the formation of defects and the overall porosity of the material. Different solvents can have varying solubility for the metal ions and organic linkers, leading to differences in crystal size, morphology, and surface area [20]. Solvents possessing high boiling point and low vapor pressure, such as dimethylformamide (DMF) or N,N'-dimethylacetamide (DMA) facilitate slow and controlled crystal growth, resulting in large and more well-defined MOF-5 crystals. On the other hand, using solvents with low boiling points, such as ethanol or methanol, can lead to faster nucleation and growth kinetics resulting in smaller crystal sizes, higher defect densities, and increased surface area. These factors can directly influence the photocatalytic property of MOF-5.

The reaction temperature during synthesis also plays an important role in controlling the rate of crystal nucleation and growth. Higher temperatures generally promote faster crystal growth, which can lead to larger MOF-5 crystals. However, excessively high temperatures can also result in rapid crystal growth and reduced crystallinity, potentially decreasing the surface area and porosity. It has been observed that lower reaction temperatures tend to result in higher porosity and surface area due to slower crystal growth and reduced aggregation. Moreover, low reaction temperatures often lead to better stability due to slow and more controlled crystal growth. Optimal reaction temperature and solvent for MOF-5 synthesis may vary depending on the specific linker, metal ion, and solvent used [13,21]. Hence, finding the appropriate synthesis parameters is crucial to achieve the desired properties and maximize the photocatalytic performance of MOF-5 [22]. In one work, the MOF-5 was synthesized by slow diffusion and direct mixing of trimethylamine (TEA), and by using solvothermal method of synthesis [23]. Small irregular particles were obtained by slow diffusion method of TEA

and direct mixing of TEA while larger size particles were obtained by solvothermal method, which indicates that synthesis procedures influence the morphology of the synthesized materials. Similarly, MOF-5 was prepared by solvothermal method and electrochemical synthesis process [24]. The former method shows regular cubic morphology while the latter method results in spherical structure, thereby indicating that the morphology of the materials greatly depends on the synthesis methods. Degradation ratio of organic dye Methyl Orange is 65.44% and 87.9% when MOF-5 synthesized with solvothermal method and electrochemical method were combined with BiOBr, which in turn shows that the synthesis methods strongly impact photocatalytic behavior of the material as well.

Considering the noteworthy photocatalytic properties of Zn-based MOFs and their sensitivity towards synthesis conditions, the present work focuses on synthesizing MOF-5 by varying reaction temperature and solvents. The three samples were synthesized through a chemical mixing method employing a magnetic stirrer. The first sample (M1) was synthesized using dimethylformamide (DMF) solvent and triethylamine (TEA) at 50 °C. The second sample (M2) was synthesized using DMF and TEA at room temperature, while the third sample (M3) was synthesized using N-methyl-2-pyrrolidone (NMP) as a solvent at room temperature. The impact of processing parameters on the different properties of the material was studied and finally their application as a photocatalyst for MB degradation is assessed. It is interesting to find that the change in morphology and elemental content has remarkable effect on photocatalytic activity of the material for dye degradation phenomenon. This work emphasizes the usability of MOF-5 for dye degradation and the effect of different synthesis methods on its performance.

2. Materials and Methods

2.1 Materials

Zinc acetate dihydrate, terephthalic acid, triethylamine (TEA), chloroform, NMP was purchased from Central Drug House (P) Ltd. (CDH), India and DMF was purchased from Fisher Scientific, India. Methylene blue was purchased from Qualikems Fine Chem Pvt. Ltd, India. All the chemicals were used as received without any further purification.

2.2 Synthesis of MOF-5

MOF-5 was synthesized using chemical synthesis method by following previously described procedure with some modification [25,26]. The three samples were synthesized by varying temperature and solvent. The first sample was synthesized using DMF solvent and at elevated temperature of 50 °C, while the second sample was prepared using same solvent but at room temperature. Upon successful synthesis of the second sample at room temperature, the replacement of DMF with NMP was also analyzed. Therefore, the third sample was synthesized at room temperature with NMP**.** In the first method, 2.125 g zinc acetate dihydrate was added to 60 mL of DMF and 0.643 g terephthalic acid was added to 50 mL of DMF. The two solutions were mixed along with the addition of 1.2 mL of TEA as capping agent. The mixture was stirred for 15 min to get white precipitates. The reaction was stirred additionally for 2 h at a temperature of 50 °C and kept still for 48 h before decanting the supernatant. The obtained precipitates were washed by immersing them overnight in DMF. Again, the DMF was decanted, and the precipitates were immersed in chloroform for 7 days and the solvent was exchanged once after 2nd, 3rd and then 7th day. The white powder was dried in an oven at 50 °C for 4-5 h. The sample obtained using this method is named M1.

In the second method, the reaction mixture obtained after the addition of TEA (same as for the sample M1 - 2.125 g zinc acetate dihydrate added to 60 mL of DMF, and 0.643 g terephthalic acid added to 50 mL of DMF, and 1.2 mL of TEA as capping agent) was stirred for 45 min at room temperature without heating. Precipitates were washed with the same process described above. The sample prepared using method 2 is named as M2. In the third method, 0.2 g zinc acetate was dissolved in 30 ml NMP and 0.543 g terephthalic acid was dissolved in 80 mL NMP. Zinc acetate solution is added to terephthalic acid solution drop by drop. The obtained solution is stirred magnetically for 10 min. Then the solution is kept at room temperature for 72 h. The precipitates were washed with NMP and dried at 120 ℃ for 12 h in oven. The obtained sample is named M3.

2.3 Characterization Techniques

Absorption spectra of all the three samples were taken using a Shimadzu UV-3600i Plus UV-VIS-NIR spectrophotometer in 200-800 nm wavelength range. The absorption spectrum of

MOF-5 was recorded using distilled water as reference. The powdered samples were characterized at ambient temperature. The structural analysis of MOF-5 samples was carried out via a Rikagu Miniflex 600 X-ray Diffractometer using Cu-Kα radiation source. Scanning electron microscope (SEM), JCM-7000 NeoScope, was used for morphological characterization of the samples. RAMAN spectra and Photoluminescence measurements of samples were recorded using WITec–ALPHA300 RAS microscope with 355 nm laser source. TGA was carried out using Shimadzu TGA–50 Series Thermogravimetric Analyzers to compare the thermal stability of the materials.

2.4 Photocatalytic Activity

In the present work, 30 mg of catalyst was dissolved in 50 mL aqueous solution of MB (20 mg/L). The solution mixture was stirred in the dark for 30 min to acquire adsorption-desorption equilibrium. Then the solution was irradiated with sunlight using solar simulator (Ossila Ltd.) with a beam power of 100 mW per cm^2. Small amount of sample was withdrawn from the mixture to note the absorption spectra using UV-Visible spectrometer at regular interval of time. Absorption spectra was taken in wavelength range of 200 to 900 nm at different time intervals for all the three samples. The above process was repeated to acquire the data for dye degradation under dark conditions.

3. Results and Discussion

3.1 Optical Properties

The MOF-5 samples synthesized with different parameters were characterized using UV-Visible spectroscopy. The UV-visible spectra can provide insights into the optical properties and electronic structure of the material. The choice of solvent and temperature can affect the structure and properties of the resulting material, including its absorption characteristics. The absorption spectra of all three samples (Figure 1) shows a sharp increment in absorption near 280 nm. The samples absorb strongly in the UV range and no shift in peaks is observed when comparing the three samples. The MOF-5 samples show slight variation in the amount of absorption from 300-800 nm with M2 having highest absorption followed by M1 and M3. Moreover, it can be discerned from the spectra that samples prepared in DMF show higher absorption as compared to NMP solvent. The enhanced absorption of light can be attributed to the stronger interactions of DMF with the MOF-5 structure due to its polar nature. The solvation effects of DMF on the MOF-5 may result in increased electronic transitions or stabilization of energy levels, leading to higher absorbance.

The bandgap (E_g) of MOF-5 samples was determined using the Tauc's relation for direct bandgap materials:

$$(\alpha h\upsilon)^2 = K(h\upsilon - E_g) \quad (1)$$

where, α, K, and υ are the coefficient of absorption, a constant of proportionality, and the photon frequency, respectively. The bandgap value of M1, M2, and M3 is 4.10 eV, 3.98 eV and 4.14 eV, respectively [27,28]. Variation in band gap was observed with change in reaction conditions which is in the order as M3 > M1 > M2. The low value of band gap of the material leads to more absorption as observed for samples M1,

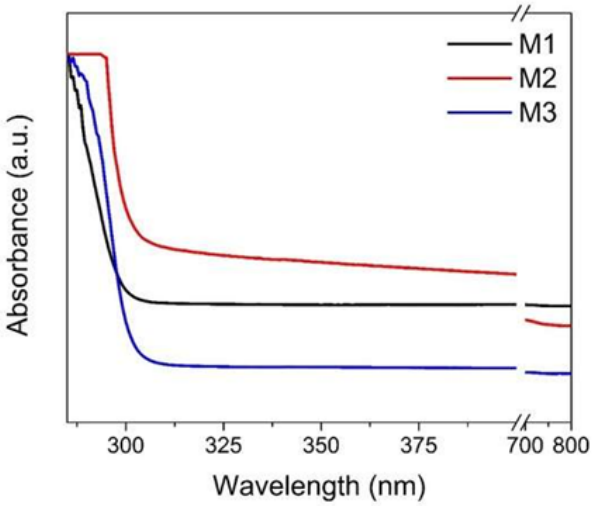

Figure 1. Absorption spectra of M1, M2, and M3.

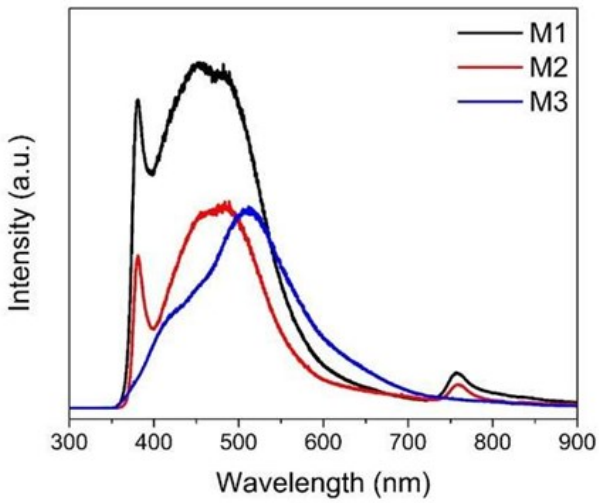

Figure 2. Emission spectra at 355 nm of M1, M2, and M3.

M2 and M3. Also, the rise in the absorption (absorption edge) starts at higher wavelength for M2 sample, which means the bandgap of M2 is lower than the other two samples. So, the amount of absorption and the position of the absorption edge, both correlate well with the calculated bandgaps. Lowest value of band gap might cause greatest degradation performance as depicted by methylene blue degradation results shown later in this article.

For understanding the catalytic behavior of MOF-5, the analysis of photoluminescence spectra was also carried out. Figure 2 shows the photoluminescence emission spectra of MOF-5 samples at an excitation wavelength of 355 nm. M1 and M2 emission spectra show three emission peaks. For M1, a sharp emission peak occurs at 380 nm, a broad and most intense peak occurs at 455 nm, and a low intensity peak occurs at 758 nm. Similarly, the three peaks for M2 appear at 382 nm, 475 nm, and 760 nm. The emission peak of M1 and M2 at ~380 nm in ultraviolet region is attributed to the electron-hole recombination caused by the zinc and oxygen vacancy defects. The broad peak at ~455 nm is related to the excitonic recombination caused by oxygen vacancy defects, and the small intensity peak around ~760 nm arises due to the frequency multiplication of the excitation source wavelength (355 nm) [29]. Emission peak at 760 nm in the near infrared region might also be attributed to excess oxygen and zinc interstitials [30]. It can be seen from UV-Visible and PL spectra that upon excitation MOF-5 emits light in the region of lesser absorption. The spectrum of M3 consists of a broad photoluminescence peak at ~508 nm along with a shoulder peak at ~417 nm, while the third peak is missing. The clear red shift of the peak positions may be attributed to morphological differences caused by the different preparation processes. The shift of peak of M3 to longer wavelength as compared to M1 and M2 may be the result of adsorbed water molecules. From the emission spectra, it is observed that PL intensity of M3 is smaller than M1 and M2 indicating lower recombination of electron and hole pairs.

3.2 Structural Properties

The FTIR spectra of the three samples are shown in Figure 3. For sample M1, the peaks at 1375 and 1580 cm^{-1} are due to symmetric and asymmetric stretching vibrations of carboxylate anion −COO− from BDC linker, respectively. Peak at 1016 cm^{-1} arises from the in-plane vibration present in the BDC spectra [31]. The bands at 745 and 821 cm^{-1} can be attributed to the aromatic C−H out-of-plane deformation vibrations in 1,4, disubstituted rings of BDC linker. Two additional bands at 480 and 655 cm^{-1} are also observable, which indicate ZnO stretching vibration. Peak at 3606 cm^{-1} occurs because of O−H stretch of non-bonded hydroxyl group. The peak positions for sample M2 are observed at 3606, 1584, 1373, 1017, 814, 748, 651and 459 cm^{-1} which are almost at the same position as that of M1. The peaks of sample M3 are located at 1624, 1385, 823, 750 and 545 cm^{-1}. Peak at 1624 cm^{-1} may correspond to C=O stretching band of NMP, and the peak located at 1385 cm^{-1} is due to asymmetric stretching of −COO− group of carboxylic acid. The peak positions between 700-1200 cm^{-1} correspond to terephthalate compounds, while the peak at 545 cm^{-1} is characteristic of ZnO molecule [32].

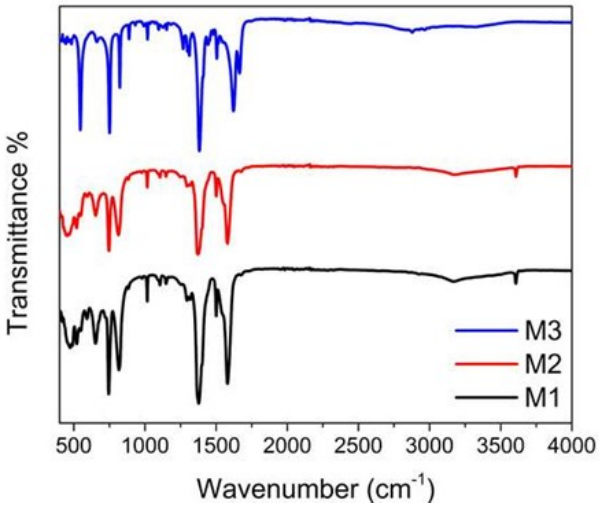

Figure 3. FTIR spectra of M1, M2 and M3.

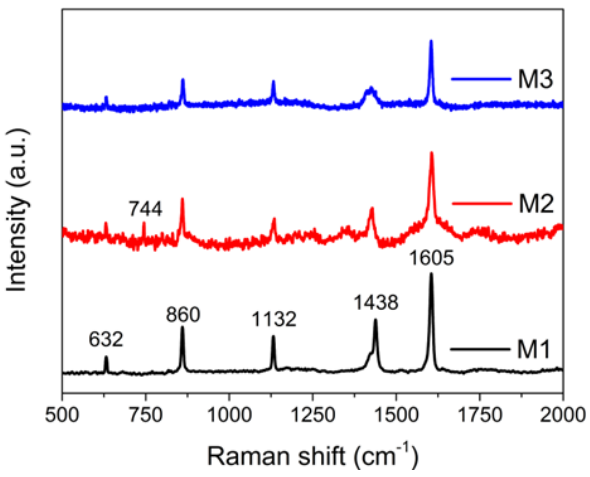

Figure 4. Raman spectra of M1, M2 and M3.

Figure 4 displays the Raman spectra of the three samples of MOF-5. The spectrum displays bands related to the vibrations of the framework, which are influenced by the metal clusters and their coordination environment.

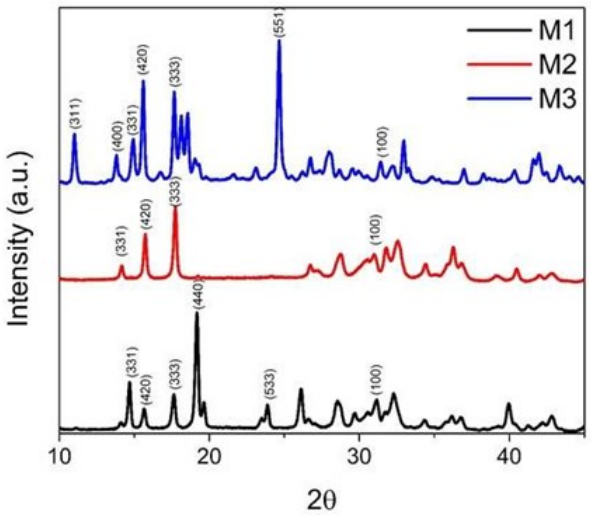

Figure 5. XRD pattern for M1, M2, and M3.

These bands can provide insights into the structural stability and the nature of metal-ligand bonding within the framework. The noticeable peaks of M1 are at 633, 861, 1133, 1440, and 1606 cm^{-1}. The peaks at 633 and 861 cm^{-1} are attributed to the out-of-plane deformation modes of the C–H bond [33,34]. Peaks at 1133 and 1440 cm^{-1} result from in-plane vibrations of benzene ring and the peak at 1606 cm^{-1} correspond to C=O stretching of the carboxylate group [35]. For M2, the Raman shifts occur at 630, 744, 860, 1134, 1427, and 1606 cm^{-1}, while for M3, the peaks are located at 632, 862, 1132, 1422, and 1604 cm^{-1}. The appearance of peak at 744 cm^{-1} in M2 sample may be assigned to in-plane bending of C–C in terephthalic acid [36]. M1 sample shows intense spectra which may be due to the geometry of the crystals formed as a result of the elevated temperature. M1 is synthesized at comparatively higher temperature than M2 and M3 and show wafer like structure as depicted through SEM images.

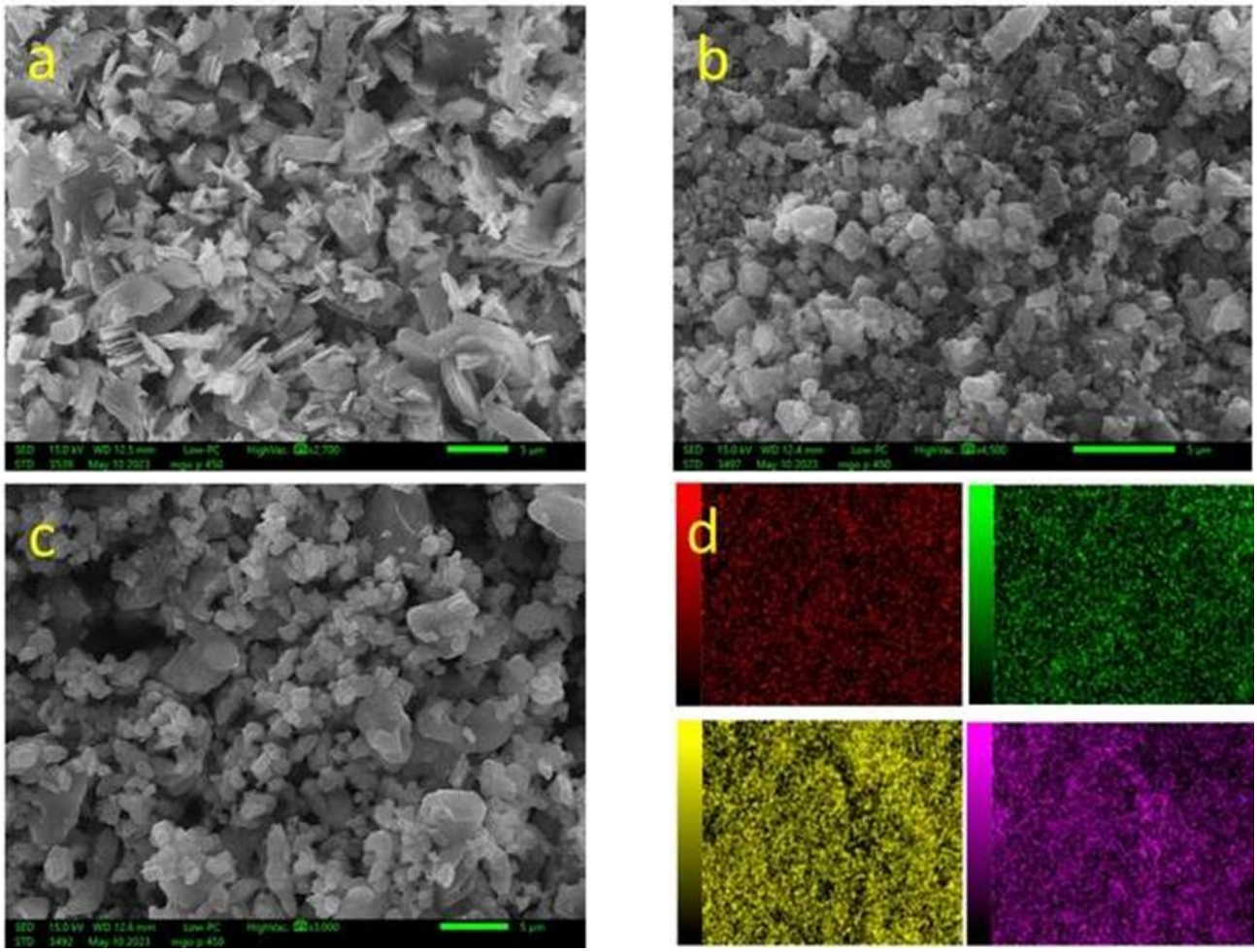

Figure 6. SEM images of (a) M1, (b) M2, (c) M3, and (d) elemental mapping of M1 sample depicting uniform distribution of carbon (red), nitrogen (green), oxygen (yellow), and zinc (purple).

The XRD pattern for all the three samples is shown in Figure 5. JCPDS No. 96-432-6738 was used for the analysis of the XRD pattern. The main peaks of M1 are situated at 14.67°, 15.76°, 17.59°, 19.18°, 26.19°, 32.38°, and 39.96°. Similar peaks are observed for M2 and occur at 14.14°, 15.74°, 17.76°, 26.8°, 28.8°, 38.52°, 36.26°, and 45.36°. Peaks at 15.76°, 17.59°, 19.18°, and 26.19° indicate the formation of MOF-5 [37]. The slight variation in main peak positions in the range of 10° to 20° arise due to change in morphology of the material due to variation in temperature and solvent [38,39]. Other higher peaks between 30° to 50° show the presence of small amount of ZnO. The peaks of M3 appear at 11.02°, 15.62°, 17.64°, 24.62°, 33.00°, and 41.94°. Differences in relative peak intensities and unidentified peaks are indication of interpenetrated frameworks. Exposure to environment cause distortion in structure which might be responsible for additional peaks [40].

The crystallite size (D), lattice microstrain (ε), and dislocation density (δ) are calculated from the XRD data of all the three samples. The average crystallite size is computed using Scherrer equation:

$$D = \frac{k\lambda}{\beta \cos\theta} \tag{2}$$

where, λ = wavelength of incident x-rays, k = size factor, θ = Bragg's angle, and β = full width at half maximum. The average crystallite size for M1, M2, and M3 are 30.6 nm, 24.2 nm, and 38.8 nm, respectively, as analyzed by Debye-Scherrer equation. Williamson-Hall (WH) method is used for determining the intrinsic strain along with dislocation density. The microstrain values obtained are 2.19×10^{-3}, 6.14×10^{-3} and 0.49×10^{-3} for M1, M2 and M3, respectively. The positive value of microstrain indicates tensile strain or lattice expansion [41] and directly correlate with the particle size as well [42]. The dislocation density of M1, M2 and M3 are 10.6×10^{10}, 17.07×10^{10} and 6.6×10^{10}, respectively, as given in Table 1.

3.3 Morphological Properties

Figure 6 shows the SEM images of the samples, and it provides valuable information about their morphology. The morphology of the three samples synthesized at the different reaction conditions are quite different. M1 contains sheet and wafer-like particles, while M2 shows cubic morphology along with different sized particles. M3 shows irregularly shaped particles with more well-defined boundaries. The SEM image shows that the particles of M3 sample have smooth surface and voids between the particles. The different geometries result from the synthesis conditions adopted for the samples. Figure 6(d) shows the elemental mapping of sample M1 from which it is clear that MOF-5 is composed of Zn, C, N, and O, and the different elements are distributed uniformly. The elemental composition in mass % of the three samples is tabulated in Table 1. The amount of Zn is maximum in M2, followed by M1 and M3 as shown in EDX spectra (Figure 7). It has been demonstrated that the interactions and transformations of zinc ions within

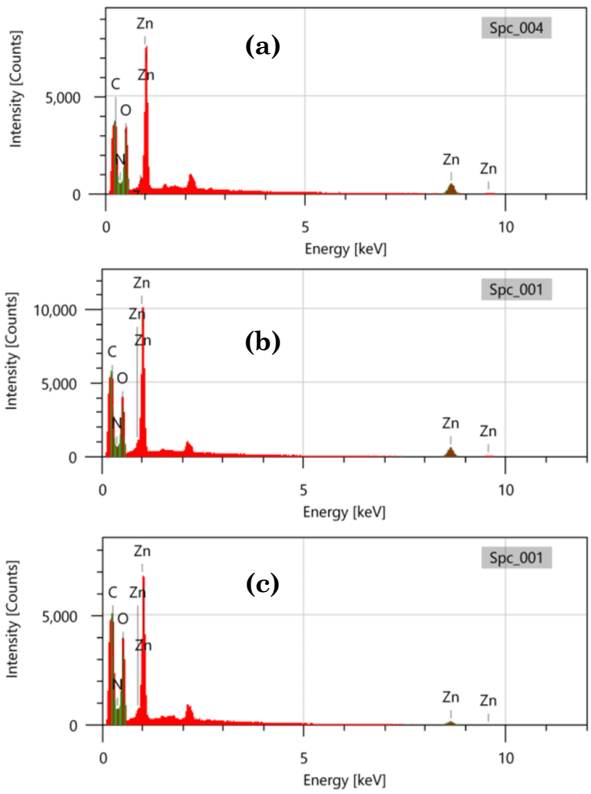

Figure 7. EDX spectra of (a) M1, (b) M2, and (c) M3.

Table 1. Optical bandgap, structural parameters and elemental composition of MOF-5 samples.

Sample	E_g (eV)	D (nm)	ε ($\times10^{-3}$)	δ (line/cm^2)	Zn (mass %)	C (mass %)	N (mass %)	O (mass %)
M1	4.10	30.6	2.19	10.6×10^{10}	48.97	14.04	5.87	31.13
M2	3.98	24.2	6.14	17.07×10^{10}	59.91	13.90	5.16	21.03
M3	4.14	38.8	0.49	6.6×10^{10}	34.42	17.51	9.64	38.35

the material are contingent upon MOF-5's capacity to undergo distortion [43]. Therefore, it is conceivable that the facilitation of zinc ion binding to MOF-5 nodes is more readily achieved when utilizing DMF as a solvent compared to NMP. Also, nitrogen and oxygen content increases in the order M3>M1>M2. The amount of nitrogen and oxygen content influences the catalytic/photocatalytic properties of materials as discussed in Section "Dye degradation".

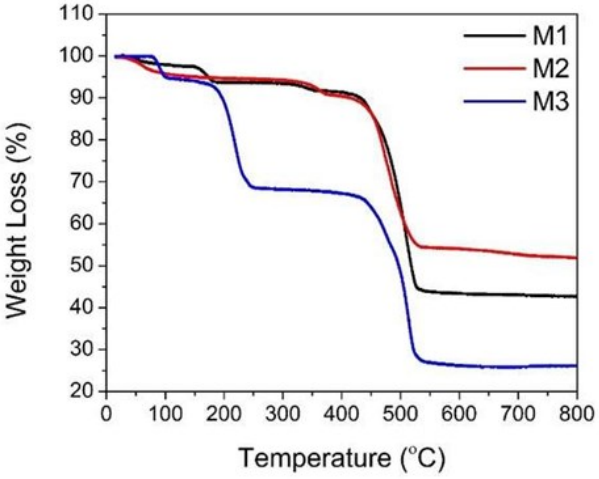

Figure 8. Thermogravimetric curves of M1, M2, and M3.

3.4 Thermal Properties

Thermogravimetric analysis (TGA) of all the three samples is carried out to assess the change in weight with temperature and is shown in Figure 8. For M1, there are two weight loss processes before 200 °C. The weight loss of ~2.5% between 15 to 150 °C is caused by the loss of moisture from the sample. A weight loss of about 3% occurs between 150 to 175 °C, which can be associated with the removal of residual DMF solvent. A significant weight loss of about 45.7% takes place between 425 to 530 °C, which can be attributed to decomposition of

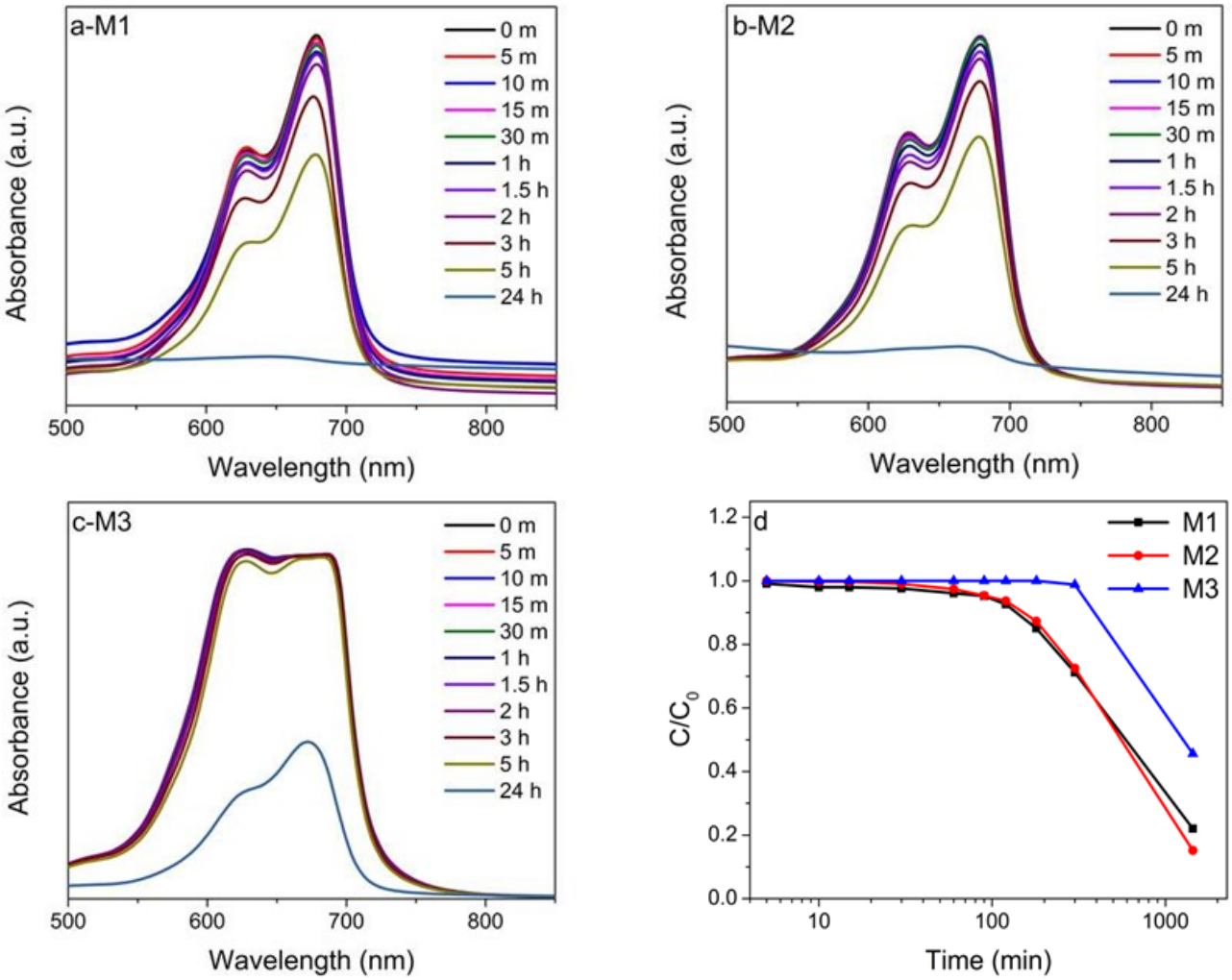

Figure 9. Photocatalytic degradation of methylene blue by (a) M1, (b) M2, (c) M3, and (d) C/C_0 versus time graph.

the sample and at 530 ℃ the sample decomposes completely [44].

The TG curve of M2 displays three weight loss processes. A weight loss of 2% up to 100 ℃ occurs from the loss of moisture from the sample. Second weight loss of 2% up to 340 ℃ may arise from the loss of DMF and traces of TEA [45]. The dramatic weight loss of 34% indicates the collapse of the framework starting from 435 ℃ up to 530 ℃. The TGA curve of M3 also shows three weight loss regions. The weight loss of 4.7% below 100 ℃ is due to the loss of moisture from the framework, weight loss of 24% from 180 to 250 ℃ is due to evaporation of the solvent NMP in the framework, while weight loss of 40% from 425 to 530 ℃ indicates the collapse of the framework [46]. All the samples decompose completely at 530 ℃. It can be seen from the graph that M3 sample is not thermally stable as compared to M1 and M2. The reduced thermal stability of M3 sample can be due to the difficulty in removing DMF from the pores of the other two sample as compared to NMP solvent in M3, which affects the degradation process.

3.5 Dye Degradation

Methylene Blue (MB) is a common organic dye, and it is highly challenging to decompose it from wastewater. The photocatalytic activity of the MOF-5 samples is analyzed by exposing the MB solution containing photocatalyst to light radiation using solar simulator. Degradation of MB is tracked by its characteristic absorption peak at 678 nm. Absorption intensity versus wavelength graphs are plotted (Figure 9(a-c)) at different times for the MOF-5 catalyst. There is a decrease in the peak intensities of absorption spectra indicating the decomposition of the organic pollutant. Percentage of degradation is calculated using:

$$Degradation\,(\%) = \frac{C_0 - C}{C_0} \times 100 \qquad (3)$$

where, C_0 = initial concentration of MB and C = concentration of MB at time t. The degradation of MB is 78% after 24 h of adding the catalyst M1. Degradation of MB caused by catalyst M2 is 85% after 24 h, while the addition of M3 as catalyst shows only 54% degradation up to 24 h. Although M1 starts degrading the dye earlier than the other two MOFs but M2 leads to the highest degradation rate after 24 h. Figure 9(d) shows the catalytic degradation efficiency plot (C/C_0 vs. time) of the MOF-5. Initially, dye is degraded at slow rate but degradation rate significantly increases with time. Decrease in the value of C/C_0 with time for all the samples indicates that MB is degraded in the presence of sunlight and it can be concluded that degradation performance of M2 is better than M1 and M3. Comparison of degradation performance of MB dye by the MOF-5 under light and dark conditions is shown in Figure 10(a), where the efficacy of the photocatalyst is clearly established and Figure 10(b) shows the schematic diagram for mechanism of photocatalytic degradation of MB by MOF-5.

The decomposition of MB using MOF-5 may be explained considering MOFs as semiconductors or photocatalysts with bandgaps dictated by the gap between the organic ligand molecules' highest occupied molecular orbital (HOMO) and lowest unoccupied molecular orbital (LUMO). Upon irradiation, the electrons (e^-) will be stimulated from the HOMO to the LUMO when exposed to photons having energy equal to or higher than the bandgap of MOFs, leading to the generation of holes (h^+) in the HOMO. The electron gets transferred to the Zn^{2+} of MOF-5 resulting in formation of Zn^+ and terephthalate radical monoanion as shown

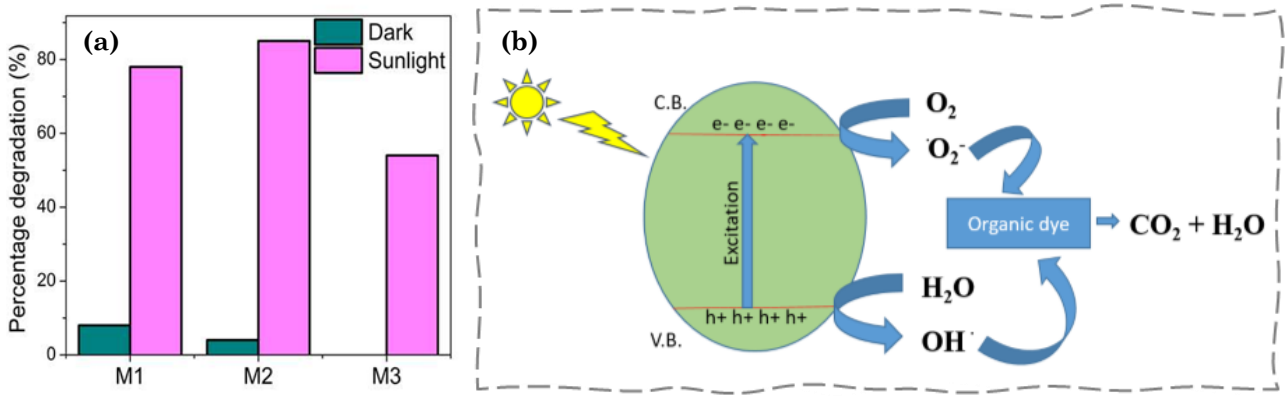

Figure 10. (a) Comparison of degradation of MB after 24 hours under dark and light conditions. (b) Schematic diagram for mechanism of photocatalytic degradation of MB by MOF-5.

in Figure 11(a) [47]. This charge transfer occurs through ligand-to-metal charge transfer (LMCT) and is thought to be the mechanism that allows MOFs to undergo photocatalysis [48].

Further, the MB dye molecules may get adsorbed onto MOF-5 via (i) electrostatic interaction of the positive charge on N and S atom of MB dye with the negative charge on π-bond of benzene ring in MOF-5, (ii) π-π interaction between the aromatic rings of the two materials, and (iii) hydrogen bonding between the H atom in MB and the O atom in MOF-5 [49]. The different interaction pathways are shown in Figure 11(b).

The adsorbed MB dye may now degrade following the mechanism shown in Figure 11(c). The holes have a significant oxidation capacity and may either directly oxidize adsorbed organic substances or interact with hydroxyl ions to produce hydroxyl radicals (•OH). The created •OH radicals cleave the C−S^+=C in MB leading to S=O and thereafter N−H_2 bond. The superoxide radicals (•O^{2-}), which are formed when photogenerated electrons get captured by oxygen molecules, have a significant oxidizing activity, and may degrade MB molecules in harmless products through sequential reactions as reported in literature [50–52]. This entire mechanism may be understood from the following reactions (Equations (4)-(7)).

$$\text{MOF-5} + h\nu \rightarrow h^+ + e^- \quad (4)$$

$$e^- + O_2 \rightarrow \cdot O_2^- \quad (5)$$

$$h^+ + OH^- \rightarrow \cdot OH \quad (6)$$

$$h^+, \cdot O_2^-, \cdot OH + MB \rightarrow CO_2 + H_2O \quad (7)$$

The photocatalytic activity of M1, M2 and M3 can be explained based on the properties of the three samples. The wafer-like morphology of M1 provides suitable open space for the MB solution to penetrate. A higher surface area of M1 exposes the dye solution to more active sites leading to good photocatalytic degradation of MB. On the other hand, M2 has smaller yet wide distribution of particle size due to which the effective surface area is high. The M3 sample has somewhat larger particle sizes with uncompact surface features, thereby showing reduced photocatalytic behavior. The TGA data also shows that M3 sample is unstable as compared to M1 and M2. Since NMP is used for the preparation of M3, the M3 particles homogeneously dissolved in the dye solu-

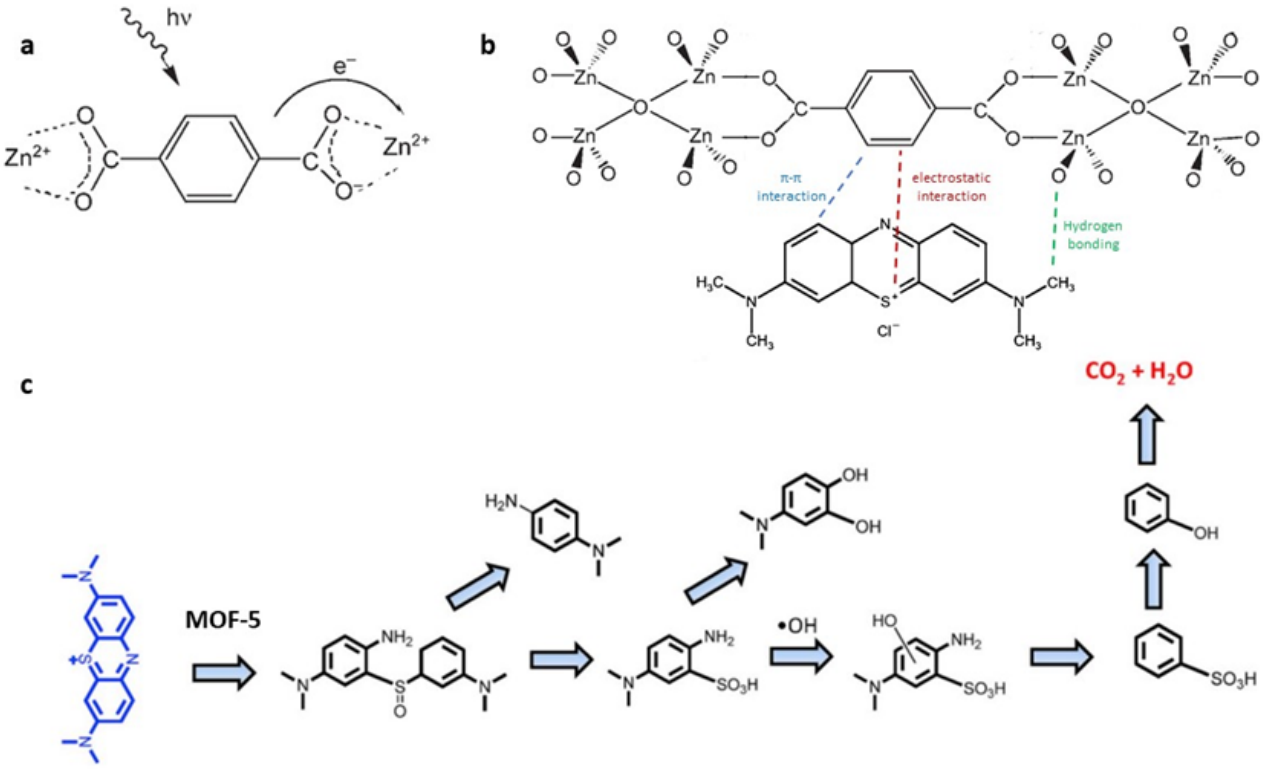

Figure 11. (a) Absorption of light by the ligand of MOF-5 and charge transfer to the metallic site. Adapted from [47] Copyright © 2007 by Wiley (b) Various possible interactions of the methylene dye molecule with MOF-5. Adapted from [49] Copyright © 2022 by BCREC Group under the CC BY-SA License (c) Degradation steps of the methylene blue dye into unharmful products. Adapted from [50], Copyright © 2020 Elsevier.

tion and led to the lowest amount of degradation.

In terms of the composition, M2 has the highest amount of Zn which is responsible for the photocatalysis. The metal ions primarily contribute to photodegradation by promoting charge separation and facilitating charge transfer leading to generation of reactive oxygen species. These reactive species are responsible for breaking down organic dyes. The findings are further supported by the PL spectrum where it is observed that the PL peak is quenched in case of M2 as compared to M1. Quenching of the peak conveys that the electron-hole recombination is lower in M2. Moreover, M2 shows higher absorption in the visible region.

Although studies have shown that the presence of nitrogen and oxygen is useful for catalytic activity, it is solely dependent on the amount and nature of the functional groups. In the present case, M1 and M2 hold optimum amount of nitrogen content, while it increases for M3, and thus, a reduction in the catalytic activity is observed for M3 [46]. Further the oxygen content is considerably high in M3 as compared to M1 and M2. During photocatalysis, excess nitrogen can trap the photoinduced electrons, preventing them from participating in the redox reactions. The excess oxygen content can react with the photogenerated charges, thereby inhibiting the reaction with dye molecules and reducing the efficiency of the photocatalyst.

4. Conclusions

In summary, three samples of MOF-5 have been prepared using simple and efficient chemical synthesis methods using different temperature and solvent and used for degradation of MB organic dye under sunlight using solar simulator. It has been observed that there is slight variation in optical and structural properties of the material with change in temperature and solvent. UV-Visible spectra depict a decrease in bandgap for sample M2 as compared to M1 and M3, which is also verified by PL spectra. However, substantial differences in the morphology of the samples is observed with change in the synthesis conditions. The photocatalytic degradation amount of 78% and 85% is obtained after 24 hours of adding the catalyst M1 and M2, respectively, while 54% degradation is observed by the catalyst M3. Thus, the highest degradation of MB in the presence of sunlight occurs for the sample prepared using DMF solvent without heating. This may be attributed to the higher Zn content in M2, more absorption in the visible range, and optimum amount of nitrogen and oxygen species.

CRediT Author Statement

All authors contributed to the study conception and design. Material preparation, data collection and analysis were performed by *Himanshi, Isha Saini,* and *Vinamrita Singh*. Reviewing and characterization were done by *Tanuj Kumar* and *Varsha Singh*. The first draft of the manuscript was written by *Himanshi* and all authors commented on previous versions of the manuscript. All authors read and approved the final manuscript.

References

[1] Widiyandari, H., Al Ja'farawy, M.S., Parasdila, H., Astuti, Y., Arutanti, O., Mufti, N., (2023). Temperature impact on the morphological evolution of nitrogen-doped carbon quantum dot-decorated zinc oxide and its influence on highly efficient visible-light photocatalyst. *Physica B: Condensed Matter.*, 669, 415293. DOI: 10.1016/j.physb.2023.415293.

[2] Mahmoodi, N.M., Abdi, J. (2018). Nanoporous metal-organic framework (MOF-199): Synthesis, characterization and photocatalytic degradation of Basic Blue 41. *Microchemical Journal*, 144, 436-442. DOI: 10.1016/j.microc.2018.09.033.

[3] Husain, Q. (2006). Potential Applications of the Oxidoreductive Enzymes in the Decolorization and Detoxification of Textile and Other Synthetic Dyes from Polluted Water : A Review. *Critical Reviews in Biotechnology*, 26, 201-221. DOI: 10.1080/07388550600969936.

[4] Ajmal, A., Majeed, I., Malik, R.N., Idrissc, H., Nadeem, M.A. (2014). Principles and mechanisms of photocatalytic dye degradation on TiO2 based photocatalysts: a comparative overview. *RSC Advances*, 4, 37003-37026, DOI: 10.1039/C4RA06658H.

[5] Chai, W.S., Cheun, J.Y., Kumar, P.S., Mubashir, M., Majeed, Z., Banat, F., Ho, S., Show, P.L. (2021). A review on conventional and novel materials towards heavy metal adsorption in wastewater treatment application. *Journal of Cleaner Production*, 296, 126589. DOI: 10.1016/j.jclepro.2021.126589.

[6] Deng, D., Aouad, W., Braff, W. A., Schlumpberger, S., Suss, M. E., Bazant, M.Z. (2015). Water purification by shock electrodialysis : Deionization , filtration , separation , and disinfection. *Desalination.* 357, 77-83, DOI: 10.1016/j.desal.2014.11.011.

[7] Wetchakun, K., Wetchakun, N., Sakulsermsuk, S. (2018). An overview of solar/visible light driven heterogeneous photocatalysis for water purification: TiO2- and ZnO-based photocatalysts used in suspension photoreactors. *Journal of Industrial and Engineering Chemistry*, 71, 19-49. DOI: 10.1016/j.jiec.2018.11.025.

[8] Yayuk, A., Fauzan, M., Arnelli, A., Iis, N., (2022). French Fries-Like Bismuth Oxide: Physicochemical Properties, Electrical Conductivity and Photocatalytic Activity. *Bulletin of Chemical Reaction Engineering & Catalysis*, 17(1), 146-156. DOI: 10.9767/bcrec.17.1.12554.146-156.

[9] Singh, P., Abdullah, M.M., Ikram, S. (2016). Role of Nanomaterials and their Applications as Photo-catalyst and Senors: A Review. *Nano Research & Applications*, 2, 1-10.

[10] Qasem, K.M.A., Khan, S., Chinnan, S., Saleh, H.A.M., Mantasha, I., Zeeshan, M., Manea, Y.K., Shahid, M. (2022). Sustainable fabrication of Co-MOF@CNT nano-composite for efficient adsorption and removal of organic dyes and selective sensing of Cr (VI) in aqueous phase. *Materials Chemistry and Physics*, 291, 126748. DOI: 10.1016/j.matchemphys.2022.126748.

[11] Tranchemontagne, D.J., Hunt, J.R., Yaghi, O.M. (2008). Room temperature synthesis of metal organic frameworks: MOF-5, MOF-74, MOF-177, MOF-199, and IRMOF-0. *Tetrahedron*, 64, 8553-8557, DOI: 10.1016/j.tet.2008.06.036.

[12] Zulys, A., Adawiah, A., Gunlazuardi, J., Yudhi, M.D.L. (2021). Light-Harvesting Metal Organic Frameworks (MOFs) La-PTC for Photocatalytic Dyes Degradation. *Bulletin of Chemical Reaction Engineering & Catalysis*, 16(1), 170-178. DOI: 10.9767/bcrec.16.1.10309.170-178.

[13] Mckinstry, C., Cathcart, R.J., Cussen, E.J., Fletcher, A.J., Patwardhan S.V., Sefcik, (2016). Scalable continuous solvothermal synthesis of metal organic framework (MOF-5). *Crystals*, 285, 718-725. DOI: 10.1016/j.cej.2015.10.023.

[14] Yap, M.H., Fow, K.L., Chen, G.Z. (2017). Synthesis and applications of MOF derived porous nanostructures. *Green Energy & Environment*, 2, 218-245. DOI: 10.1016/j.gee.2017.05.003.

[15] Wang, Q., Gao, Q., Al-enizi A.M. (2020). Recent advances in MOF-based photocatalysis : environmental remediation under visible light. *Inorganic Chemistry Frontiers,* 7, 300-339. DOI: 10.1039/C9QI01120J.

[16] Zhao, D., Cai, C. (2021). Dyes and Pigments Cerium-based UiO-66 metal-organic framework for synergistic dye adsorption and photodegradation : A discussion of the mechanism. *Dye Pigment,* 185, 108957. DOI: 10.1016/j.dyepig.2020.108957.

[17] Zhang, T.Q.S., Wang, M., Zeng, L., Zhou, H., Pana, Z., Qingrong, C. (2018). Two pure MOF-photocatalysts with readily preparation for the degradation of methylene blue dye under visible light. *Dalton Transactions,* 47, 4251-4258. DOI: 10.1039/C8DT00156A.

[18] Pan, Y., Ding, Q., Singh C.S.A., Kumar, A., Liu, J. (2019). A new Zn(II)-based 3D metal-organic framework with uncommon sev topology and its photocatalytic property for the degradation of organic dyes. *CrystEngComm*, 21, 4578-4585. DOI: 10.1039/C9CE00759H.

[19] Devarayapalli, K.C., Vattikuti, S.V.P., Tvm, S., Yoo, K.S., Nagajyothi, P.S., Shim, J. (2019). Facile synthesis of Ni-MOF using microwave irradiation method and application in the photocatalytic degradation. *Materials Research Express,* 6, 1150h3. DOI: 10.1088/2053-1591/ab5261.

[20] Bugaz, E., Erciyes, A., Andac, M. (2019). Inorganic Chemica. Acta. Synthesis and characterization of nano-sized metal organic framework-5 (MOF-5) by using consecutive combination of ultrasound and microwave irradiation methods. *Inorganica Chimica Acta,* 485, 118-124. DOI: 10.1016/j.ica.2018.10.014.

[21] Mckinstry, C., Cussen, E.J., Fletcher, A.J., Patwardhan, S.V., Sefcik, J. (2013). Effect of Synthesis Conditions on Formation Pathways of Metal Organic Framework (MOF-5). *Crystal Growth & Design,* 13, 5481-5489. DOI: 10.1021/cg4014619.

[22] Younis, S.A., Kwonc, E.E., Qasim, M., Kima, K., Kimd, T., Kukkar, D., Douf, X., Ali, I. (2020). Metal-organic framework as a photocatalyst: Progress in modulation strategies and environmental/energy application. *Progress in Energy and Combustion Science*, 81, 100870. DOI: 10.1016/j.pecs.2020.100870.

[23] Li, J., Cheng, S., Zhao, Q., Long, P., Dong, J., (2009). Synthesis and hydrogen-storage behavior of metal – organic framework MOF-5. *International Journal of Hydrogen Energy,* 34, 1377-1382. DOI: 10.1016/j.ijhydene.2008.11.048.

[24] Yang, H., Liu, X., Song, X., Yang, T., Liang, Z., Fan, C. (2015). In situ electrochemical synthesis of MOF-5 and its application in improving photocatalytic activity of BiOBr. *Transactions of Nonferrous Metals Society of China*, 25, 3987-3994. DOI: DOI: 10.1016/S1003-6326(15)64047-X.

[25] Reza, M., Negar, M., Ashouri, M.F. (2018). Nitrate Adsorption from Aqueous Solution by Metal – Organic Framework MOF-5. *Iranian Journal of Science and Technology, Transactions A: Science*, 43, 443-449. DOI: 10.1007/s40995-017-0423-6.

[26] Umezawa, S., Douura, T., Yoshikawa, K., Tanaka, D., Stolojan, V., Ravi, S., Silva, P., Yoneda, M., Gotoh, K. (2023). Zinc-based metal-organic frameworks for high-performance supercapacitor electrodes: Mechanism underlying pore generation. *Energy & Environmental Materials*, 6, e12320. DOI: 10.1002/eem2.12320.

[27] Fiaz, M., Kashif, M., Fatima, M., Rabia, S., Muhammad, B., Asghar, A. (2020). Synthesis of Efficient TMS @ MOF - 5 Catalysts for Oxygen Evolution Reaction. *Catalysis Letters,* 150, 2648-2659. DOI: 10.1007/s10562-020-03155-6.

[28] Ataei, F., Dorranian, D., (2021). Synthesis of MOF-5 nanostructures by laser ablation method in liquid and evaluation of its properties. *Journal of Materials Science: Materials in Electronics,* 32, 3819-3833. DOI: 10.1007/s10854-020-05126-4.

[29] Yang, S.J., Im, J.H., Kim, T., Lee, K., Park, C.R. (2011). MOF-derived ZnO and ZnO@C composites with high photocatalytic activity and adsorption capacity. *Journal of Hazardous Materials,* 186, 376-382. DOI: 10.1016/j.jhazmat.2010.11.019.

[30] Zhang, Y., Lan, D., Wang, Y., Cao, H., Jiang, H. (2011). MOF-5 decorated hierarchical ZnO nanorod arrays and its photoluminescence. *Physica E: Low-dimensional Systems and Nanostructures*, 43, 1219-1223. DOI: 10.1016/j.physe.2011.02.004.

[31] Biserčić, M.S., Marjanović, B., Vasiljević, B.N., Mentus, S., Zasońska, B.A., Ćirić, marjanović, G. (2019). Quest for optimal water quantity in the synthesis of metal-organic framework MOF-5. *Microporous and Mesoporous Materials*, 278, 23-29. DOI: 10.1016/j.micromeso.2018.11.005.

[32] Zhang, S., Li, D., Guo, D., Zhang, H., Shi, W., Cheng, P., Wojtas, L., Zaworotko, M.J. (2015). Synthesis of a Chiral Crystal Form of MOF-5, CMOF-5, by Chiral Induction. *Journal of the American Chemical Society*, 137, 15406-15409. DOI: 10.1021/jacs.5b11150.

[33] Rather, R.A., Siddiqui, Z.N. (2019). Silver phosphate supported on metal–organic framework (Ag_3PO_4@MOF-5) as a novel heterogeneous catalyst for green synthesis of indenoquinolinediones. *Applied Organometallic Chemistry*, 33, e5176. DOI: 10.1002/aoc.5176.

[34] Bordiga, S., Lamberti, C., Ricchiardi, G., Regli, L., Bonino, F., Damin, A., Lillerud, K.P., Bjorgenb, M., Zecchina, A. (2004). Electronic and vibrational properties of a MOF-5 metal organic framework : ZnO quantum dot behaviour. *Chemical Communications,* 5, 2300-2301. DOI: 10.1039/B407246D.

[35] Saha, D., Deng, S. (2010). Ammonia adsorption and its effects on framework stability of MOF-5 and MOF-177. *Journal of Colloid and Interface Science*, 348, 615-620. DOI: 10.1016/j.jcis.2010.04.078.

[36] Mahalakshmi, G., Balachandran, V. (2014). FT-IR and FT-Raman spectra, normal coordinate analysis and ab initio computations of Trimesic acid. *Spectrochimica Acta Part A: Molecular and Biomolecular Spectroscopy,* 124, 535-547, DOI: 10.1016/j.saa.2014.01.061.

[37] Yang, H.M., Song, X.L., Yang, T.L., Liang, Z.H., Fan, C.M., Hao, X.G. (2014). Electrochemical synthesis of fl ower shaped morphology MOFs in an ionic liquid system and their electrocatalytic application to the hydrogen evolution reaction. *RSC Advances,* 4, 15720-15726. DOI: 10.1039/C3RA47744D.

[38] Lua, C., Liub, J., Xiao, K., Harris, A.T., (2010). Microwave enhanced synthesis of MOF-5 and its CO_2 capture ability at moderate temperatures across multiple capture and release cycles. *Chemical Engineering Journal*, 156, 465–470. DOI: 10.1016/j.cej.2009.10.067.

[39] Manzoor, U., Zahra, F.T., Rafique, S., Moin, M.T., Mujahid, M. (2015). Effect of Synthesis Temperature, Nucleation Time, and Postsynthesis Heat Treatment of ZnO Nanoparticles and Its Sensing Properties. *Journal of Nanomaterials*, 2015, 189058. DOI: 10.1155/2015/189058.

[40] Wang, S., Xie, X., Xia, W., Cui, J., Zhang, S., Du, X. (2020). Study on the structure activity relationship of the crystal MOF-5 synthesis , thermal stability and N_2 adsorption property. *High Temperature Materials and Processes*, 39, 171-177. DOI: 10.1515/htmp-2020-0034.

[41] Priya, B., Jasrotia, P., Kumar, A., Singh, V., Kumar, T. (2022). Structural, optical, and electrical properties of V_2O_5 thin films : Nitrogen implantation and the role of different substrates. *Frontiers in Materials*, 9, 1-13, DOI: 10.3389/fmats.2022.1049189.

[42] Murugesan, C., Chandrasekaran, G. (2015). Impact of Gd^{3+} substitution on the structural, magnetic and electrical properties of cobalt ferrite nanoparticles. *RSC Advances,* 5, 73714-73725. DOI: 10.1039/C5RA14351A.

[43] Brozek, C.K., Michaelis, V.K., Ong, T., Bellarosa, L., Lopez, Griffin, R.G., Dinca, M. (2015). Dynamic DMF Binding in MOF-5 Enables the Formation of Metastable Cobalt-Substituted MOF-5 Analogues. *ACS Central Science*, 1, 252-260. DOI: 10.1021/acscentsci.5b00247.

[44] Chen, B., Wang, X., Zhang, Q., Xi, X., Cai, J., Qi, H., Shi, S., Wang, J., Yuan, D., Fang, M. (2010). Synthesis and characterization of the interpenetrated MOF-5. *Journal of Materials Chemistry*, 20, 3758-3767. DOI: 10.1039/B922528E.

[45] Chatterjee, A., Jana, A.K., Basu, J.K. (2020). Silica supported binary metal organic framework for removing organic dye involving combined effect of adsorption followed by photocatalytic degradation. *Materials Research Bulletin,* 138, 111227. DOI: 10.1016/j.materresbull.2021.111227.

[46] Wang, J., Tafen, D.N., Lewis, J.P., Hong, Z., Manivannan, A., Zhi, M., Li, M., Wu, N., (2009). Origin of Photocatalytic Activity of Nitrogen-Doped TiO2 Nanobelts. *Journal of the American Chemical Society*, 131, 12290-12297. DOI: 10.1021/ja903781h.

[47] Alvaro, M., Carbonell, E., Ferrer, B., Xamena, F.X.L., Garcia H. (2007). Semiconductor Behavior of a Metal-Organic Framework (MOF). *Chemistry – A European Journal*, 13, 5106–5112. DOI: 10.1002/chem.200601003.

[48] Tong, Y., Li, Y., Sun, L., Yang, R., Zhang, S., Fu, Y., Cao, L., Chen, R. (2020). The prominent photocatalytic activity with the charge transfer in the organic ligand for $[Zn_4O(BDC)_3]$ MOF-5 decorated Ag_3PO_4 hybrids. *Separation and Purification Technology,* 250, 117142. DOI: 10.1016/j.seppur.2020.117142.

[49] Adawiah, A., Oktavia, W., Saridewi N., Azhar F.M., Fitria R.N., Gunawan M.S., Komala S., Zulys A. (2022). Synthesis Metal-Organic Framework (MOFs) Cr-PTC-HIna Modulated Isonicotinic Acid for Methylene Blue Photocatalytic Degradation. *Bulletin of Chemical Reaction Engineering & Catalysis*, 17(2), 383-393. DOI: 10.9767/bcrec.17.2.13930.383-393.

[50] Angel, L., Herrera, A., Reyes, P.K.C., Flores, A.M.H., Martínez, L.T., Villanueva, J.M.R., (2020). BDC-Zn MOF sensitization by MO/MB adsorption for photocatalytic hydrogen evolution under solar light. *Materials Science in Semiconductor Processing*, 109, 104950. DOI: 10.1016/j.mssp.2020.104950.

[51] Yao, T., Tan, Y., Zhou, Y., Chen, Y., Xiang, M. (2022). Preparation of core-shell MOF-5/Bi_2WO_6 composite for the enhanced photocatalytic degradation of pollutants. *Journal of Solid State Chemistry,* 308, 122882. DOI: 10.1016/j.jssc.2022.122882.

[52] Sathya, M., Selvan, G., Karunakaran, M. (2023). Synthesis and characterization of cadmium doped on ZnO thin films prepared by SILAR method for photocatalytic degradation properties of MB under UV irradiation. *The European Physical Journal Plus,* 138, 67. DOI: 10.1140/epjp/s13360-023-03667-1.